A Finite Element Model of Flatfoot (Pes Planus) for Improving Surgical Plan

Zhongkui Wang[1], Kan Imai[2], Masamitsu Kido[2], Kazuya Ikoma[2], and Shinichi Hirai[1]

Abstract— **Flatfoot is a foot condition caused by the collapse of the medial arch of the foot, and it can result in problems such as severe pain, swelling, abnormal gait, and difficulty walking. Despite being a very common foot deformity, flatfoot is one of the least understood orthopaedic problems, and the opinions regarding its optimal treatment vary widely. In this paper, an FE model of a flatfoot is proposed that is based on CT measurements. Surface meshes of the bones and soft tissue were generated from CT images and then simplified to reduce the node density. A total of 62 ligaments, 9 tendons, and the plantar fascia were modeled manually. Volume meshes of the different components were generated and combined to form the completed flatfoot model. A dynamic FE formulation was derived, and a balanced standing simulation was performed. The model was validated by comparing stress distribution results from the simulation to experimental data.**

I. INTRODUCTION

Flatfoot (also called Pes Planus) is a very common and chronic foot deformity that is characterized by a loss of arch height, hindfoot valgus, and forefoot abduction when the foot is loaded. Patients with flatfoot may develop lower extremity pain, swelling, abnormal gait, and difficulty walking. There are various causes of flatfoot, including posterior tibial tendon (PTT) dysfunction (*e.g.*, rupture, attenuation, or laceration), midfoot laxity, external rotation of the hindfoot, trauma (*e.g.*, lisfranc, talonavicular joint, or calcaneus injuries), and neuromuscular imbalance [1]. Although flatfoot is a very common foot deformity, it remains one of the least understood, and optimal treatment is not widely accepted [2].

To study the biomechanics of flatfoot, experimental and computational models have been investigated in the literature. In experimental studies, cadaver feet from healthy human have generally been used, rather than flatfeet, because of the limitation of donors. Flatfoot models were generated by releasing or sectioning specific ligaments and tendons [3], [4]. However, these artificially created flatfeet may not accurately mimic realistic ligament functions because people with flatfeet have attenuated but still functioning ligaments. To address this problem, Blackman *et al*. created an artificial flatfoot model by attenuating specific ligaments [5]. However, they only attenuated the ligaments up to 17500 cycles, due to time limitations. This attenuation is inadequate considering that adult acquired flatfoot is over years. An additional limitation of the experimental models is that the bone shapes and configurations may be different in healthy feet and flatfeet. In clinical cases, medical doctors tend to have varying opinions regarding the optimal surgery for an individual patient. It is difficult to use one specimen to investigate the optimal surgery, because performing multiple surgeries on the same patient is not generally feasible.

As a result of the aforementioned limitations, computational models, *e.g.*, specifically finite element (FE) models, have been studied. However, very few FE models of flatfoot have been published to date. The only FE flatfoot model found in the literature was developed by Lewis to perform surgical simulations [2]. This model consisted of 14 bone segments, 65 ligaments, and part of the plantar soft tissue. However, the toes and dorsal soft tissue were not included. Other than FE models, a rigid-body flatfoot model was proposed by Spratley *et al*. for studying the kinematic behavior of the flatfoot skeleton [6].

In addition to flatfoot, FE models of healthy feet have been developed for various applications. Cheung *et al*. presented an FE foot model based on MR images. This model was used to study the effects of soft tissue stiffening on the stress distribution of the plantar surface during balanced standing [7]. The same model was also used to study the biomechanical effects of different types of foot orthosis for improving design principles [8]. A foot-boot model was built by Qiu *et al*. for the future study of foot wear design and parachute landing impact for the military [9]. FE foot models were also proposed for studying clawed hallux deformity [10] and for developing ankle prosthesis [11].

All of the above-mentioned models were developed using commercial FE software packages. Specifically, ABAQUS® was used in [2], [7], [8] and [11]; ANSYS® was used in [9]; and LS-DYNA® was used in [10]. In these studies, ligaments, tendons, and plantar fascia were modeled as 1D elements, which is nonrealistic because these tissues occupy 3D volume. It is particularly unrealistic for the plantar fascia, which occupy a relatively large area on the bottom of the foot. Thus, simplifying it into 1D element may affect the stress distribution on the foot bottom.

In this paper, we propose a dynamic FE model of a flatfoot that is based on computed tomography (CT) data. Free software packages were used to edit the surface meshes and generate volume meshes. Dynamic FE equations were formulated and implemented in MATLAB®. Ligaments, tendons, and the plantar fascia were created manually as 3D elements. While not using commercial FE software led to some dif-

*This work was supported in part by Grant-in-Aid for Scientific Research (No. 2324604), and also by MEXT KAKENHI 26860404, JSPS, Japan.

[1]Zhongkui Wang and Shinichi Hirai are with the Department of Robotics, Ritsumeikan University, 525-8577 Shiga, Japan {wangzk at fc and hirai at se}.ritsumei.ac.jp

[2]Kan Imai, Masamitsu Kido, and Kazuya Ikoma are with the Department of Orthopaedics, Kyoto Prefectural University of Medicine, 602-8566 Kyoto, Japan{kan-imai, masamits, kazuya}at koto.kpu-m.ac.jp

978-1-4244-7929-0/14/$26.00 ©2014 IEEE

ficulty (*e.g.*, with preprocessing and postprocessing), it also provided more possibilities and freedom with using custom-defined functions and materials. The developed model will be used in future studies to simulate surgical operations and further realize tailor-made surgery for individual patients.

II. MESH GENERATION

A. Surface Mesh Generation and Simplification

The flatfoot (right foot) geometry was obtained from a 3D reconstruction of CT images obtained from a male patient who was 38 years old and 168 cm tall and weighed 62 kg. During CT measurement, a custom-made foot loading device was used to fix the patient's lower limb, as described in [12]. The CT images of the bones and soft tissue were reconstructed into 3D surface meshes using Mimics® (Materialise Inc., Leuven, Belgium). The CT measurements and segmentations were performed by foot and ankle surgeons from Kyoto Prefecture University of Medicine, and the measurements were approved by an ethics committee at the University. The surface meshes were subsequently imported into a free software package named Meshlab® (http://meshlab.sourceforge.net/) for editing. To reduce the computational cost in the FE simulation, the surface meshes were simplified to reduce the number of nodes. The simplified surface meshes, which include 17 bones and soft tissue, are shown in Fig. 1.

B. Creation for the Ligaments, Tendons, and Plantar Fascia

From CT images, it is difficult to discriminate ligaments, tendons, and the plantar fascia from the surrounding soft tissue. Therefore, geometrical meshes of ligaments, tendons, and the plantar fascia were created manually by referring to [13] and following the recommendations of foot and ankle surgeons. First, we located the origin and insertion positions of a ligament and then selected several nodes on the bone surfaces to approximate the origin and insertion positions. These nodes were then connected to one another to construct a surface mesh that represented the ligament. Using this method, a total of 62 ligaments, 9 tendons, and the plantar fascia were created (Fig. 2).

C. Volume Tetrahedral Mesh Generation

The surface meshes of all components were saved as '.obj' files, which included the information for the nodal coordinates and triangular connections. These data were used to create '.poly' files, which were then invoked by an open-source mesh generator, 'TetGen' (http://wias-berlin.de/software/tetgen/), to generate volume tetrahedral meshes. The tetrahedral mesh of soft tissue that was generated is shown in Fig. 3 as an example. The nodes on the internal surface of the soft tissue (bone caves in Fig. 3) had the same coordinates as the nodes on the bone surfaces. This ensured good connections between the bones and soft tissue during assembly. Cartilage tissue was not included in the current model. Instead, the gaps between neighboring bones were filled with soft tissue. Tetrahedral meshes of all components were combined to construct a complete flatfoot model containing a total of 13830 nodes and 66051 tetrahedral elements.

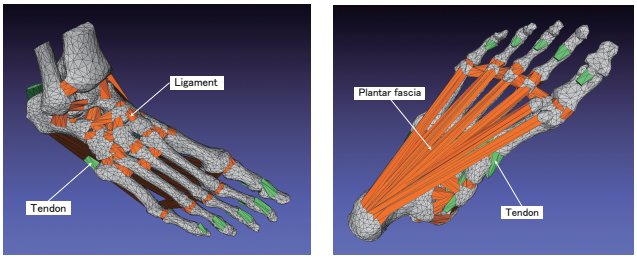

Fig. 2. The created ligaments, tendons, and the plantar fascia in (a) dorsal view and (b) plantar view

III. DYNAMIC FE FORMULATION

The FE formulation followed process similar to that presented in our previous paper [14]. The bone components were modeled as a linear elastic material, and the other components were modeled as viscoelastic (Voigt model in [14]) materials. The mechanical properties used for all of the components are given in Table I, where the superscript denotes the reference number. Notably, the Young's moduli of bone, ligament, and plantar fascia listed in Table I have been widely used in other foot models. Most researchers have modeled soft tissue as a hyperelastic material without a Young's modulus. In [7], [8], [9], [10], and [11], tendons were implicitly modeled by applying forces on several nodes of the corresponding bone surfaces without using mechanical properties. In this paper, we explicitly modeled 9 tendons using the experimentally measured Young's modulus reported by [15], [16]. Due to the lack of references on viscous moduli, we manually set $c = 100\,\mathrm{Pa{\cdot}s}$ to reduce the amount

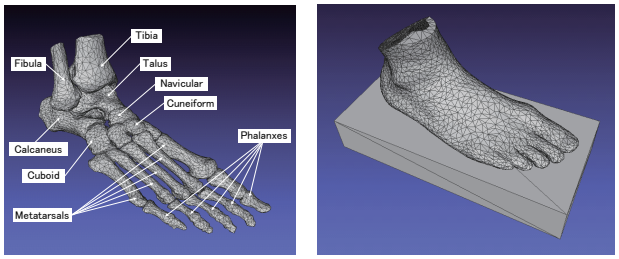

Fig. 1. The surface meshes of (a) bones and (b) soft tissue and ground

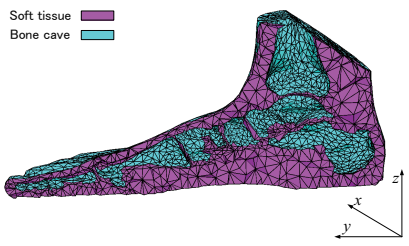

Fig. 3. The cross-section view of the soft tissue mesh

TABLE I

THE MATERIAL PROPERTIES USED IN THE FE MODEL

Component	Density (Kg/m^3)	Young's modulus (MPa)	Viscous modulus (Pa·s)	Poisson's ratio
Bone	449[10]	7300[7]−[9],[11]	0	0.3[7]−[11]
Ligament	1000	260[7]−[9],[11]	100	0.4[9],[11]
Tendon	1000	1500[15],[16]	100	0.4
Fascia	1000	350[7]−[9],[11]	100	0.4[9],[11]
Soft tissue	1000[10]	2.49[10]	100	0.49[10]

of vibration during the simulation.

To assemble all of the components and derive the dynamic FE equations, we calculated global stiffness and viscous matrices, which implicitly represented the connections between different components. We first calculated the local stiffness matrix $\boldsymbol{K}_i^{ela}$ of a component with its own properties as

$$\boldsymbol{K}_i^{ela} = \lambda_i^{ela}\boldsymbol{J}_\lambda^i + \mu_i^{ela}\boldsymbol{J}_\mu^i, \tag{1}$$

where i denotes the i-th component, λ^{ela} and μ^{ela} are Lamé's constants, defined by Hooke's law, and $\boldsymbol{J}_\lambda$ and $\boldsymbol{J}_\mu$ are connection matrices that only depend on the original coordinates of the mesh nodes. Similarly, a local viscous matrix was calculated as

$$\boldsymbol{K}_i^{vis} = \lambda_i^{vis}\boldsymbol{J}_\lambda^i + \mu_i^{vis}\boldsymbol{J}_\mu^i, \tag{2}$$

where λ^{vis} and μ^{vis} describe the material viscosity [14].

Global stiffness and viscous matrices, $\boldsymbol{K}^{ela}$ and $\boldsymbol{K}^{vis}$, were then formulated by assembling all of the local matrices, according to the matrix assembling process of the general FE method. The global matrices included not only the geometrical connections between components but also the material properties of the different components. Following a derivation similar to that presented in [14], a set of differential equations for simulating the dynamic behavior of the flatfoot was formulated as follows:

$$\begin{aligned} \dot{\boldsymbol{u}}_N &= \boldsymbol{v}_N, \\ \boldsymbol{M}\dot{\boldsymbol{v}}_N - \boldsymbol{A}\mathscr{L} &= -(\boldsymbol{K}^{ela}\boldsymbol{u}_N + \boldsymbol{K}^{vis}\boldsymbol{v}_N) + \boldsymbol{F}_{tendon}, \\ -\boldsymbol{A}^{\mathrm{T}}(\dot{\boldsymbol{v}}_N - \ddot{\boldsymbol{u}}_c) &= \boldsymbol{A}^{\mathrm{T}}[2\omega(\boldsymbol{v}_N - \dot{\boldsymbol{u}}_c) + \omega^2(\boldsymbol{u}_N - \boldsymbol{u}_c)], \end{aligned} \tag{3}$$

where N denotes the number of nodes, the vectors $\boldsymbol{u}_N$ and $\boldsymbol{v}_N$ consist of three components of displacement and velocity for all nodes, $\boldsymbol{M}$ is the inertia matrix, and $\boldsymbol{F}_{tendon}$ consists of the pull forces acting on all tendons. Gravity is neglected. The pulling forces on the tendons during balanced standing were not found in the literature. Instead, the pulling forces on tendons during mid-stance, reported in [17] for a body weight of 683 N, were used. Because the body weight of our subject was 62 kg, we were able to calculate the tendon forces in our model. The calculated forces are listed in Table II. The third equation in Eq. 3 describes a set of constraints or boundary conditions using CSM [18]. In a balanced standing simulation, the boundary conditions are to fix the top surfaces of the tibia and fibula bones. Therefore, the vector $\boldsymbol{u}_c$ is equal to zero here. If $\boldsymbol{u}_c$ were a displacement function of the ankle during a gait cycle, a walking simulation would be performed. Constant ω is a predetermined angular frequency and was set to $1000\,\mathrm{s}^{-1}$ in the simulation. The vector $\mathscr{L}$ is a set of Lagrange multipliers describing the constraint reaction forces. The matrix $\boldsymbol{A}$ denotes the nodes that need to be constrained. The ground (Fig. 1b) was modeled as a rigid block and was pushed upward by an external force (equal to body weight) during the simulation.

TABLE II

THE PULL FORCES ON TENDONS USED IN THE MODEL

Tendon	Force (N)	Tendon	Force (N)
Achilles	132.53	Flexor hallucis longus	13.34
Posterior tibialis	26.68	Flexor digitorum longus	6.67
Anterior tibialis	0	Extensor hallucis longus	13.34
Peroneus longus	21.35	Extensor digitorum longus	6.67
Peroneus brevis	10.67		

Contact between the flatfoot and the ground was modeled using a traditional penalty method. Briefly, when any node on the bottom area of the flatfoot penetrates the ground, the penetration distance δ_i is calculated. A virtual penalty force $\boldsymbol{F}_i^{pen}$ was calculated to prevent the penetration as

$$\boldsymbol{F}_i^{pen} = p^{coef} \times E^{tissue} \times \delta_i, \tag{4}$$

where p^{coef} is a penalty coefficient and was set to 0.1 in the simulation, E^{tissue} is the Young's modulus of the soft tissue, and the subscript i denotes the i-th node in contact with the ground. This penalty force vector was added into the right side of the second equation of Eq. 3. Numerically solving Eq. 3 allowed us to compute the displacements and velocities of all nodes in the flatfoot model.

IV. RESULTS AND DISCUSSION

The FE model (Eq. 3) was coded and solved numerically in MATLAB®. A total of 0.1 s balanced standing simulation was performed. The stress distribution on the bottom of the foot was calculated after the simulation and compared with the experimental measurements in Fig. 4, where the dots correspond to nodes in contact with the ground and the colors denote the stress amplitude. The experimental measurements were obtained using an Emed®-M (Novel gmbH, Germany) pressure platform system. Three measurements were taken, and the average stress distribution is shown in Fig. 4b.

Figure 4 shows that the simulated contact region was similar to the measured one. The simulated rearfoot region was slightly larger, but the simulated forefoot region was a bit smaller compared with the measured data. The little-toe regions appeared in simulation but not in the measurements. High stress areas appeared in the rearfoot, mid-foot, and forefoot in the simulation but were mostly concentrated in the rearfoot area in the measurements. The peak stress in the simulation was 114.6 kPa, and the average peak stress for the measurements was 165 kPa. Published data on the peak stresses in healthy feet were found to be in a range of 131 kPa to 230 kPa [7], [9], [20], [21]. Stress data for a flatfoot were presented in [2], where the simulated peak stress was approximately 180 kPa and the measured peak

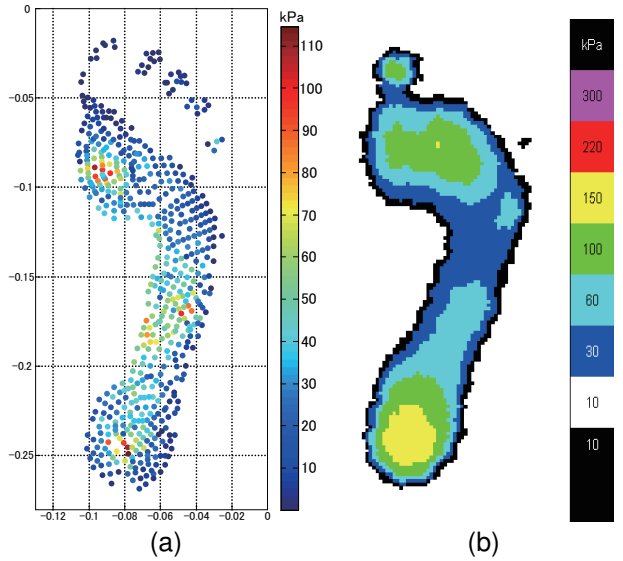

Fig. 4. The stress distributions in (a) simulation and (b) measurements

stress was between 150 kPa and 220 kPa. Clearly, our simulated peak stress was smaller than our measurement and previously published data. This difference occurred because the higher stresses were distributed over different areas in the simulation but were concentrated in the rearfoot area in the measurements. These differences between the simulation and measurements could be caused by the initial geometrical mesh. The CT measurement was taken while the patient was laying on the CT table, with his lower limb fixed by the custom-made device. During measurement, both feet were subjected to 5.7±2.6% of body weight [12], which made the bottom surfaces of the feet flat, rather than their natural curved shape. However, this initial load on the foot was not considered in the simulation. These differences could be eliminated by using a foot geometry with a natural bottom surface, which will be investigated in future work.

V. CONCLUSION

In this paper, an FE model of flatfoot was presented that was based on CT measurements. The model consisted of 17 bone segments, 62 ligaments, 9 tendons, the plantar fascia, and the soft tissue with different material properties. Bones and soft tissue were directly measured by a CT scan, but the ligaments, tendons, and plantar fascia were created manually by referring to an anatomy book and the recommendations of foot and ankle surgeons. Surface mesh editing and volume mesh generation were performed using free software packages. The FE dynamic model was formulated and programmed using MATLAB®. A balanced standing simulation was performed, and the simulated stress distribution was compared with experimental measurements and published data to validate the model. Good agreements were achieved for the contact regions, stress distributions, and peak stresses. To the best of our knowledge, this model is the first intact flatfoot model that does not use commercial FE software. The developed model will be used in future studies to simulate surgical operations, such as medializing calcaneal osteotomy and lateral column lengthening. These simulations may contribute to the development of an optimal surgery plan and the realization of a tailor-made surgery for an individual patient.

REFERENCES

[1] A. P. McCormack, R. P. Ching, and B. J. Sangeorzan, Biomechanics of Procedures Used in Adult Flatfoot Deformity, Foot and Ankle Clinics, vol. 6, no. 1, pp. 15-23, March 2001.

[2] G. S. Lewis, Computational Modeling of the Mechanics of Flatfoot Deformity and Its Surgical Corrections, Ph.D. dissertation, The Pennsylvania State University, State College, PA, 2008.

[3] H. B. Kitaoka, Z. Luo, and K. An, Three-Dimensional Analysis of Flatfoot Deformity: Cadaver Study, Foot & Ankle International, vol. 19, no. 7, pp. 447-451, 1998.

[4] W. Niu, Y. Yang, Y. Fan, Z. Ding, and G. Yu, Experimental Modeling and Biomechanical Measurement of Flatfoot Deformity, in Proc. 7th Asian-Pacific Conference on Medical and Biological Engineering (IFMBE), vol. 19, pp. 133-138, 2008.

[5] A. J. Blackman, J. J. Blevins, B. J. Sangeorzan, and W. R. Ledoux, Cadaveric Flatfoot Model: Ligament Attenuation and Achilles Tendon Overpull, vol. 27, no. 12, pp. 1547-1554, Dec., 2009.

[6] E. M. Spratley, E. A. Matheis, C. W. Hayes, R. S. Adelaar, and J. S. Wayne, Validation of A Population of Patient-Specific Adult Acquired Flatfoot Deformity Models, Journal of Orthopaedic Research, vol. 31, no. 12, pp. 1861-1868, Dec., 2013.

[7] J. T. M. Cheung, M. Zhang, A. K. L. Leung, and Y. Fan, Three-Dimensional Finite Element Analysis of the Foot During Standing–A Material Sensitivity Study, Journal of Biomechanics, vol. 38, no. 5, pp. 1045-1054, May, 2005.

[8] J. T. M. Cheung and M. Zhang, Finite Element Modeling of the Human Foot and Footwear, ABAQUS Users' Conference, pp. 145-159, 2006.

[9] T. Qiu, E. Teo, Y. Yan, and W. Lei, Finite Element Modeling of A 3D Coupled Foot-Boot Model, Medical Engineering & Physics, vol. 33, no. 10, pp. 1228-1233, Dec., 2011.

[10] V. Isvilanonda, E. Dengler, J. M. Iaquinto, B. J. Sangeorzan, and W. R. Ledoux, Finite Element Analysis of the Foot: Model Validation and Comparison between Two Common Treatments of the Clawed Hallux Deformity, Clinical Biomechanics, vol. 27, no. 8, pp. 837-844, 2012.

[11] M. Ozen, O. Sayman, and H. Havitcioglu, Modeling and Stress Analyses of A Normal Foot-Ankle and A Prosthetic Foot-Ankle Complex, Acta of Bioengineering and Biomechanics, vol. 15, no. 3, pp. 19-27, 2013.

[12] M. Kido, K. Ikoma, K. Imai, M. Maki, R. Takatori, D. Tokunaga, N. Inoue, and T. Kubo, Load Response of the Tarsal Bones in Patients with Flatfoot Deformity: In Vivo 3D Study, Foot Ankle Int., vol. 32, no. 11, pp. 1017-1022, Nov., 2011.

[13] F. H. Netter, Atlas of Human Anatomy, Fifth Edition. Elsevier, 2011, pp. 51-525.

[14] Z. Wang, L. Wang, V. A. Ho, S. Morikawa, and S. Hirai, A 3-D Nonhomogeneous FE Model of Human Fingertip Based on MRI Measurements, IEEE Transactions on Instrumentation and Measurement, vol. 61, no. 12, pp. 3147-3157, Dec., 2012.

[15] C. N. Maganaris and J. P. Paul, Rapid Report–In Vivo Human Tendon Mechanical Properties, Journal of Physiology, vol. 521, no. 1, pp. 307-313, 1999.

[16] J. Peltonen, N. J. Cronin, J. Avela, and T. Finni, In Vivo Mechanical Response of Human Achilles Tendon to A Single Bout of Hopping Exercise, The Journal of Experimental Biology, vol. 213, pp. 1259-1265, 2010.

[17] E. P. Salathe and G. A. Arangio, A Biomechanical Model of the Foot: The Role of Muscles, Thendons, and Ligaments, Journal of Biomechanical Engineering, vol.124, pp. 281-287, June 2002.

[18] J. Baumgarte, Stabilization of constraints and integrals of motion in dynamical systems, Computer Methods in Applied Mechanics and Engineering, vol.1, no.1, pp. 1-16, 1972.

[19] P. I. Kattan, MATLAB Guide to Finite Elements–An Interactive Approach, Second Edition, Springer, pp. 337-340, 2008.

[20] W. Chen, F. Tang, and C. Ju, Stress Distribution of the Foot during Mide-Stance to Push-Off in Barefoot Gait: A 3-D Finite Element Analysis, Clinical Biomechanics, vol. 16, no. 7, pp. 614-620, 2001.

[21] P. J. Antunes, G. R. Dias, A. T. Coelho, F. Rebelo, and T. Pereira, Non-Linear Finite Element Modelling of Anatomically Detailed 3D Foot Model, Online Available.